Classification of Multispectral Images Based on a Fuzzy-Possibilistic Neural Network

Jzau-Sheng Lin and Shao-Han Liu

***Abstract*—In this paper, a new Hopfield-model net based on fuzzy possibilistic reasoning is proposed for the classification of multispectral images. The main purpose is to modify the Hopfield network embedded with fuzzy possibilistic C-means (FPCM) method to construct a classification system named fuzzy-possibilistic Hopfield net (FPHN). The classification system is a paradigm for the implementation of fuzzy logic systems in neural network architecture. Instead of one state in a neuron for the conventional Hopfield nets, each neuron occupies 2 states called membership state and typicality state in the proposed FPHN. The proposed network not only solves the noise sensitivity fault of Fuzzy C-means (FCM) but also overcomes the simultaneous clustering problem of possibilistic C-means (PCM) strategy. In addition to the same characteristics as the FPCM algorithm, the simple features of this network are clear potential in optimal problem. The experimental results show that the proposed FPHN can obtain better solutions in the classification of multispectral images.**

***Index Terms*—Fuzzy-possibilistic c-means, Hopfield neural network, multispectral images, possibilistic c-means.**

I. Introduction

Multispectral classification has been described as generating better discrimination than single spectral classification [1]. In the remotely sensed images, the multispectral images are extracted from multiple-band sensors operated from either a spaceborne or an airborne platform such as Landsat seven-band Thematic Mapper (TM), four-band Multispectral Scanner (MSS), and three-band Satellite Pour 1'Observation de la Terra (SPOT). In the other words, magnetic resonance imaging (MRI) systems can produce multi-band images each of which emphasizes a different fundamental parameter of internal anatomical structures in the same body section with multiple contrasts, based on local variations of spin-lattice relaxation time (T_1), spin–spin relaxation time (T_2), and proton density (PD). The classification of multispectral images has been successfully employed in the past [1]–[8]. The analysis of such multidimensional images can be accomplished by using supervised or unsupervised classification methods. In supervised classification strategies, the region of interest (ROI) is defined by the associated human interaction and the approach trains on the ROI and flags each pixel in the scenes associated with a given signature. However, a supervised approach is very time-consuming for large volumes and heavy biases may be introduced by an unskilled technician. The unsupervised classification methods classify the multidimensional data sets without the aid of training sets, but a post-processing step is required to correct misclassified pixels.

Generally speaking, unsupervised classification approaches such as hard C-means (HCM) [9] and ISODATA [10] are traditional clustering methods in which each sample belongs only to one cluster. FCM [10]–[13], penalized FCM (PFCM) [14], [15] and compensated FCM (CFCM) [16] are called fuzzy clustering methods in which every sample belongs to all clusters with different degrees of membership. In possibilistic clustering algorithm [17], [18] every sample belongs to all clusters with different degrees of possibility. FPCM [19] solves the noise sensitivity fault of fuzzy c-means and the simultaneous clustering problem of possibilistic c-means strategy with membership and typicality.

Applications of neural-network-based approaches to pattern classification have been extensively studied in the last couple of decades. In the application of multispectral image classification, neural networks exploit the massive parallelism of neurons. Ozkan *et al.* [6] proposed a neural network-based segmentation of multi-modal medical image. To update the performance, fuzzy reasoning algorithms have been added into neural network to construct fuzzy-neural systems [7], [8], [16]. Kanstein *et al.* [20] embedded the possibilistic reasoning into a competitive learning network to clustering problem. Lin *et al.* [7], [8] presented a penalized fuzzy competitive learning network and a fuzzy Hopfield neural network (FHNN) to three-band and five-channel magnetic resonance image classification respectively. Lin [16] also embedded the compensated fuzzy c-means into Hopfield net and applied to clustering. These networks proved that better segmentation results are offered than those from a single modality. We extended the author's method in [7], [8] to multi-band image segmentation. In FHNN only one state for a neuron called membership state is used. When a training sample is classified as a proper class, membership may be a better candidate, as it is natural to assign a sample to that class whose representative vector is closest to the sample. On the other hand, when estimating cluster centers, typicality is an important constraint for alleviating the undesirable effects of outliers. In addition to the membership state in a neuron, we attempt to add other neuron state named typicality state to alleviate the undesirable effects of outliers. In this paper, the FPCM is added into Hopfield network to construct the FPHN for classification of multispectral images. This approach has two advantages, namely it is more robust to noise and it is an unsupervised algorithm based on a neural network. In order to solve the noise sensitivity in fuzzy reasoning and the simultaneous clustering problem of possibilistic learning in a neural network, the FPCM strategy is embedded into Hopfield network to construct the FPHN which can obtain more promising solutions in multispecral image classification than HCM and FHNN as shown in experimental results.

The rest of this paper is organized as follows. Section II reviews the fuzzy cluster techniques including fuzzy c-means, possibilistic c-means, and fuzzy-possibilistic c-means. Section III presents the fuzzy possibilistic Hopfield network (FPHN). Section IV shows several experimental results, and finally, Section V gives the discussion and conclusions.

II. Fuzzy Clustering Techniques

Clustering has been an indispensable paradigm to unsupervised pattern recognition. Uncertainty is largely present in multispectral images, because of the noise in acquisition and of the partial volume effects. This means that the pixel vectors, especially at the borders between volumes of interest, correspond to mixtures of different regions, because of the low resolution of sensors. As a consequence, borders between regions are not exactly defined and memberships in boundary regions are really fuzzy. In the application of mutispectral image classification, the clustering process based on fuzzy reasoning strategy is widely used. The clustering-based approaches have been shown to be more suitable to noisy images in discrimination of different regions in multispectral medical images than techniques based on edge detection [21]. In [22], a unified view of robust clustering including fuzzy and possibilistic clustering approaches were given.

Fuzzy clustering strategies are mathematical tools for detecting similarities between members of a collection of samples. The purpose of

Manuscript received August 7, 2000; revised March 26, 2001, August 30, 2001, and April 21, 2002.

The authors are with the Department of Electronic Engineering, National Chin-Yi Institute of Technology, Taichung, Taiwan, R.O.C (e-mail: jslin@chinyi.ncit.edu.tw).

Digital Object Identifier 10.1109/TSMCC.2002.807276

the FCM approach is to group data into clusters of similar items by minimizing a least squared error measure. For $c \geq 2$ and $m > 1$, the algorithm chooses $\mu_x : Z \rightarrow [0,1]$ so that $\sum_x \mu_x = 1$ for $i = 1, 2, \ldots, c$ to minimize the objective function

$$J_{\mathrm{FCM}} = \frac{1}{2} \sum_{x=1}^{n} \sum_{i=1}^{c} (\mu_{x,i})^m \| z_x - \varpi_i \|^2 \tag{1}$$

where $\mu_{x,i}$ is the value of the ith membership grade on the xth sample z_x. The cluster centers $\varpi_1, \ldots, \varpi_j, \ldots, \varpi_c$ can be regarded as prototypes for the clusters represented by the membership grades. The value $m \in [1, \infty]$ is the fuzzification parameter (or exponential weight).

FCM algorithms use the probabilistic constraint to make the memberships of a training sample with the different grades shared by distinct clusters. In contrast, each component generated by the PCM, proposed by Krishnapuram *et al.* [17], [18] for unsupervised clustering, corresponds to a dense region in the data set with a degree of typicality. In the PCM, the membership function of a point in a fuzzy set is absolute, not depending on the membership value of the same point in other clusters and each cluster is independent of the other clusters. The objective function of the PCM can be formulated as

$$J_{\mathrm{PCM}} = \frac{1}{2} \sum_{x=1}^{n} \sum_{i=1}^{c} (t_{x,i})^\eta \| z_x - \varpi_i \|^2 + \sum_{x=1}^{n} \beta_i \sum_{i=1}^{c} (1 - t_{x,i})^\eta \tag{2}$$

where β_i is the scale parameter at the ith cluster, $t_{x,i}$ is the possibilistic typicality value of training sample z_x associated with the cluster i, and $\eta \in [1, \infty)$, is a weighting factor called the possibilistic parameter. The possibilistic approach processes the membership value of a training sample in a cluster representing the typicality of the sample in the cluster, or the possibility of the sample belonging to the cluster. Each training sample is classified to only one cluster at a time rather than to all the clusters simultaneously. Therefore, a reasonable initialization is required in order to let J_{PCM} converge to the global minimum.

If a training sample is classified to a suitable cluster, membership is a better constraint for which the training sample is the closest to this cluster. In the other words, typicality is an important factor for unburdening the undesirable effects of outliers to compute the cluster centers. In accordance with [19], typicality is related to the mode of the cluster and can be calculated based on all n training samples. Thus an objective function in the FPCM, depending on both of memberships and typicalities, can be defined as

$$J_{\mathrm{FPCM}} = \frac{1}{2} \sum_{x=1}^{n} \sum_{i=1}^{c} \left(\mu_{x,i}^m + t_{x,i}^\eta \right) \| z_x - \varpi_i \|^2 \tag{3}$$

where memberships, typicalities, and centroids are

$$\mu_{x,i} = \left(\sum_{\ell=1}^{c} \frac{(\|z_x - \varpi_i\|^2)^{1/(m-1)}}{(\|z_x - \varpi_\ell\|^2)^{1/(m-1)}} \right)^{-1}; \quad x = 1, 2, \ldots, n \quad i = 1, 2, \ldots, c \tag{4}$$

$$t_{x,i} = \left(\sum_{y=1}^{n} \frac{(\|z_x - \varpi_i\|^2)^{1/(\eta-1)}}{(\|z_y - \varpi_i\|^2)^{1/(\eta-1)}} \right)^{-1}; \quad y = 1, 2, \ldots, n \quad i = 1, 2, \ldots, c \tag{5}$$

and

$$\varpi_i = \frac{1}{\sum_{y=1}^{n} \left(\mu_{y,i}^m + t_{y,i}^\eta \right)} \sum_{x=1}^{n} \left(\mu_{x,i}^m + t_{x,i}^\eta \right) z_x. \tag{6}$$

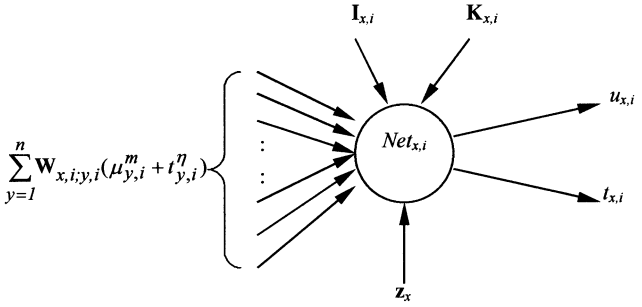

Fig. 1. Architecture of the neuron (x, i) in a 2-D FPHN.

In the FPCM, membership $\mu_{x,i}$ is a function of training sample z_x with all c cluster centers while the typicality $t_{x,i}$ is a function of training sample z_x with cluster center ϖ_i. Thus typicality $t_{x,i}$ does just depend on the location of the cluster center ϖ_i.

III. Fuzzy-Possibilistic Hopfield Neural Network

The Hopfield-model neural networks [23], [24] have been studied extensively. The features of this network are simple and have clear potential for parallel implementation. In order to improve the performance in the application of optimal problems, modified Hopfield networks [7], [8], [16], [25]–[27] have been proposed. Lin *et al.* [7], [8], [16], [26] proposed different fuzzy Hopfield networks to the applications of clustering problem and medical image segmentation. Cheng *et al.* [27] presented a possibilistic Hopfield network on CT brain hemorrhage image segmentation. These modified Hopfield networks are either based on fuzzy reasoning or possibilistic learning. In [7], [8], [16], [26], and [27], each neuron occupies only one state which is updated with a membership grade or typicality degree. For the purpose of solving the noise sensitivity fault of fuzzy reasoning and the simultaneous clustering problem of possibilistic learning, the FPCM strategy is embedded into Hopfield network to construct the FPHN in this paper. Instead of updating and memorizing the centroids for iteratively training samples in the FPCM, the neuron states and synaptic weights are updated in the modified Hofield net. Finally, the centroids are calculated using the training samples and neuron states when the energy is converged. In the FPHN, shown in Fig. 1, each neuron occupies two states named membership state based on all c cluster centers and typicality state based on all n training samples individually. In the learning process, the membership and typicality states are updated iteratively until the modified energy is converged. Thus the total weighed input for neuron (x, i) and Lyapunov energy function in the two-dimensional FPHN can be modified as

$$\mathrm{Net}_{x,i} = \left| \mathbf{z}_x - \sum_{y=1}^{n} \mathbf{W}_{x,i;y,i} \mathbf{z}_y \right|^2 + \mathbf{I}_{x,i} + \mathbf{K}_{x,i} \tag{7}$$

and

$$E = \frac{1}{2} \sum_{x=1}^{n} \sum_{i=1}^{c} \left(\mu_{x,i}^m + t_{x,i}^\eta \right) \left| \mathbf{z}_x - \sum_{y=1}^{n} \mathbf{W}_{x,i;y,i} \mathbf{z}_y \right|^2 - \sum_{x=1}^{n} \sum_{i=1}^{c} \left(\mathbf{I}_{x,i} \mu_{x,i}^m + \mathbf{K}_{x,i} t_{x,i}^\eta \right) \tag{8}$$

where $\mathbf{W}_{x,i;y,i}$ is the weighed input vector received from the neuron (y, i) at neuron (x, i), m and η are fuzzification and typicality parameters, $\mu_{x,i}$ and $t_{x,i}$ are membership and typicality states at neuron (x, i), and $\mathbf{I}_{x,i}, \mathbf{K}_{x,i}$ are input-vector biases for membership and typicality states at neuron (x, i) respectively. The minimization of (8) is under the constraints $m > 1, \eta > 1, 0 \leq \mu_{x,i}, t_{x,i} \leq 1$,

and $\sum_{i=1}^{c} \mu_{x,i} = 1\ \forall x$; and $\sum_{x=1}^{n} t_{x,i} = 1\ \forall i$. The network reaches an equilibrium state when the modified Lyapunov energy function is minimized. The objective function for clustering problem in the 2-D FPHN is defined as follows:

$$J_{\mathrm{FPHN}} = \frac{A}{2}\sum_{x=1}^{n}\sum_{i=1}^{c}\left(\mu_{x,i}^{m} + t_{x,i}^{\eta}\right) \times \left|\mathbf{z}_x - \sum_{y=1}^{n}\frac{1}{\sum_{h=1}^{n}\left(\mu_{h,i}^{m} + t_{h,i}^{\eta}\right)}\mathbf{z}_y\left(\mu_{y,i}^{m} + t_{y,i}^{\eta}\right)\right|^2 + \frac{B}{2}\left\{\left[\sum_{x=1}^{n}\sum_{i=1}^{c}(\mu_{x,i} + t_{x,i})\right] - n - c\right\}^2 \quad (9)$$

where J_{FPHN} is the objective function that accounts for the energies of all training samples in the same class, and $\mathbf{z}_x, \mathbf{z}_y$ are the training vectors at rows x and y in the FPHN, respectively.

The first term in (9) defines the Euclidean distance between the training samples in a cluster and that cluster's centers over c clusters with membership grade and typicality degree. The second term guarantees that n training samples in $\mathbf{Z}$ are distributed among these c clusters. More specifically, the second term (the constrained term), imposes constraints on the objective function, and the first term minimizes the intra-class Euclidean distance from training vectors to the cluster centers.

All the neurons in the same row compete with one another to determine the training sample represented by that row belongs to all clusters with membership grades and typicality degrees. In other words, the summation of the membership states in the same row equals to one and the summation of the typicality states in the same column also equals to one in the FPHN. That is, the total sum of membership states in all n rows equal n and the total sum of typicality states in all c columns equal c. This assures that all n samples will be classified into c classes. The objective function in this network can be further simplified as

$$J_{\mathrm{FPHN}} = \frac{1}{2}\sum_{x=1}^{n}\sum_{i=1}^{c}\left(\mu_{x,i}^{m} + t_{x,i}^{\eta}\right) \times \left|\mathbf{z}_x - \sum_{y=1}^{n}\frac{\left(\mu_{y,i}^{m} + t_{y,i}^{\eta}\right)}{\sum_{h=1}^{n}\left(\mu_{h,i}^{m} + t_{h,i}^{\eta}\right)}\mathbf{z}_y\right|^2. \quad (10)$$

By using (10), the minimization of J_{FPHN} is greatly simplified, since (10) contains only one term, the need to find the weighting factors A and B are removed. Comparing (10) with the modified Lyapunov function (8), the synaptic interconnection weights and the bias inputs for the proposed FPHN can be obtained as

$$\mathbf{W}_{x,i;y,i} = \frac{\left(\mu_{y,i}^{m} + t_{y,i}^{\eta}\right)}{\sum_{h=1}^{n}\left(\mu_{h,i}^{m} + t_{h,i}^{\eta}\right)} \quad (11)$$

$$\mathbf{I}_{x,i} = 0 \quad (12)$$

and

$$\mathbf{K}_{x,i} = 0. \quad (13)$$

By introducing (11), (12), and (13) into (7), the input of neuron (x, i) can be expressed as

$$\mathrm{Net}_{x,i} = \left|\mathbf{z}_x - \sum_{y=1}^{n}\frac{1}{\sum_{h=1}^{n}\left(\mu_{h,i}^{m} + t_{h,i}^{\eta}\right)}\mathbf{z}_y\left(\mu_{y,i}^{m} + t_{y,i}^{\eta}\right)\right|^2. \quad (14)$$

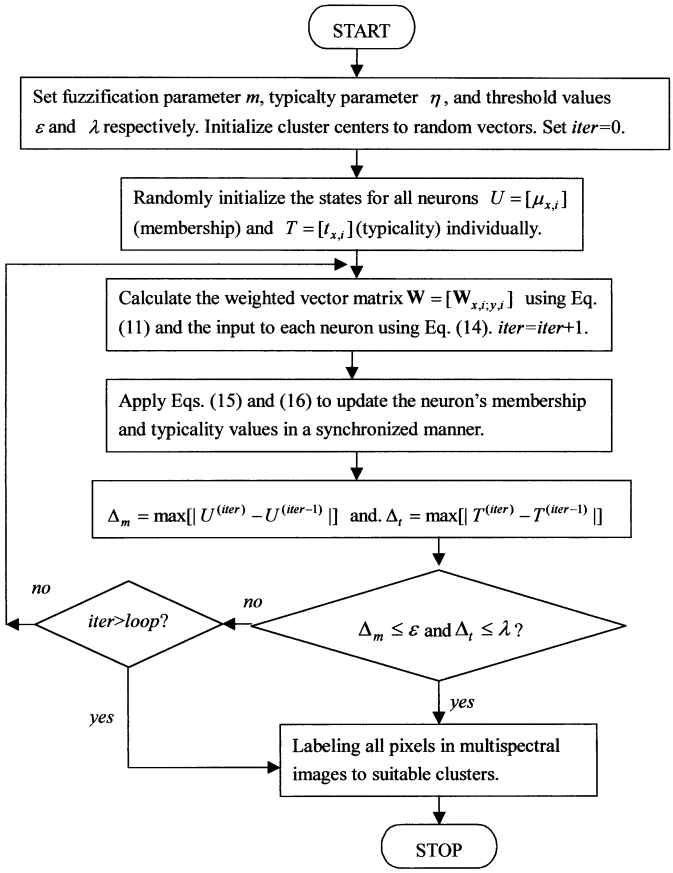

Fig. 2. Flowchart of multispectral images classification using the FPHN.

Consequently, the neuron states at neuron (x, i) in the FPHN with FPCM reasoning are given by

$$\mu_{x,i} = \left[\sum_{j=1}^{c}\left(\frac{\mathrm{Net}_{x,i}}{\mathrm{Net}_{x,j}}\right)^{1/m-1}\right]^{-1}, \quad \text{for all } i \quad (15)$$

and

$$t_{x,i} = \left[\sum_{y=1}^{n}\left(\frac{\mathrm{Net}_{x,i}}{\mathrm{Net}_{y,i}}\right)^{1/\eta-1}\right]^{-1}, \quad \text{for all } x. \quad (16)$$

Directly mapping training vectors to the 2-D neuron array, the FPHN is trained to update all neuron states in order to classify the input vectors into feasible clusters when the defined energy function converges to near global minimum. The detail process of the FPHN is shown in Fig. 2, in which parameters *iter* and *maxi* are number of iterations and maximum value of iteration respectively.

IV. Experimental Results

To show the classification performance of the FPHN, a data set proposed by Pal *et al.* [19] and two sets of al multispectral images are used for simulation in an IBM Pentium II 166 MHz computer. The data set, shown in Fig. 3, consists of 12 points on a 2-D coordinate given in Table I. Initially, the states of neurons $\mu_{x,i}$ and $t_{x,i}$ are randomly set between 0 and 1. These two states for all neurons are updated iteratively to stabilize solutions as the defined Lyapunov energy function converges to a near-global minimum value. The cluster centers associated the data set shown in Table I with $c = 2$ are $\mathbf{C}_1 = [C_{11}, C_{12}] = [(-3.1947, 0.3138), (3.1946, 0.3134)]$, $\mathbf{C}_2 = [C_{21}, C_{22}] = [(-3.2080, 0.3053), (3.2078, 0.3051)]$, and $\mathbf{C}_3 =$

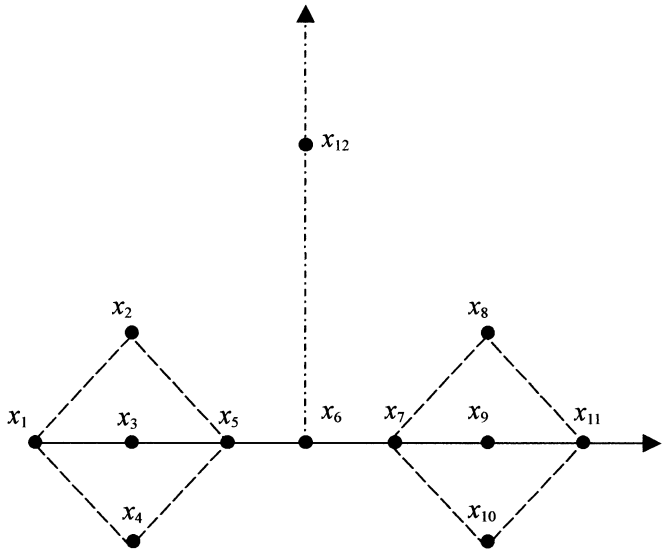

Fig. 3. Coordinates of the data set.

TABLE I
MEMBERSHIP GRADES AND TYPICALITY DEGREES FOR FCM AND FPHN

	Data set		FCM $m=3$		FHNN $m=3$		FPHN $m=3,\ \eta=3$			
x	p1	p2	$\mu_{x,1}$	$\mu_{x,2}$	$\mu_{x,1}$	$\mu_{x,2}$	$\mu_{x,1}$	$\mu_{x,2}$	$t_{x,1}$	$t_{x,2}$
1	-5.00	0.00	0.9524	0.0476	0.9465	0.0535	0.9538	0.0462	0.0227	0.0012
2	-3.34	1.67	0.9599	0.0401	0.9534	0.0466	0.9572	0.0438	0.0368	0.0015
3	-3.34	0.00	0.9972	0.0028	0.9966	0.0034	0.9976	0.0024	0.8664	0.0016
4	-3.34	-1.67	0.9218	0.0782	0.9138	0.0862	0.9249	0.0751	0.0178	0.0014
5	-1.67	0.00	0.9075	0.0925	0.8971	0.1029	0.9060	0.0940	0.0287	0.0031
6	0.0	0.00	0.5000	0.5000	0.5000	0.5000	0.5001	0.4999	0.0067	0.0067
7	1.67	0.00	0.0925	0.9075	0.1029	0.8971	0.0927	0.9073	0.0028	0.0301
8	3.34	1.67	0.0401	0.9599	0.0466	0.9534	0.0415	0.9585	0.0015	0.0385
9	3.34	0.00	0.0028	0.9972	0.0034	0.9966	0.0017	0.9983	0.0016	0.8654
10	3.34	-1.67	0.0782	0.9218	0.0861	0.9139	0.0745	0.9255	0.0014	0.0193
11	5.00	0.00	0.0476	0.9524	0.0535	0.9465	0.0456	0.9546	0.0010	0.0210
12	0.00	10.00	0.5000	0.5000	0.5000	0.5000	0.4997	0.5003	0.0005	0.0005
Class center			(-3.1947, 0.3138) (3.1946, 0.3134)		(-3.2080, 0.3053) (3.2078, 0.3051)		(-3.2045, 0.2702) (3.2048, 0.2657)			

TABLE II
INDICES OF THE 12 POINTS CORRESPONDING TO A SORT ON $t_{x,1}$ AND $t_{x,2}$

Typicality order	
$t_{x,1}$	$t_{x,2}$
3	9
2	8
5	7
1	11
4	10
6	6
7	5
9	3
8	2
10	4
11	1
12	12

$[C_{31}, C_{32}] = [(-3.2045, 0.2702), (3.2048, 0.2657)]$ generated by FCM, FHNN and FPHN respectively. The centroids were obtained

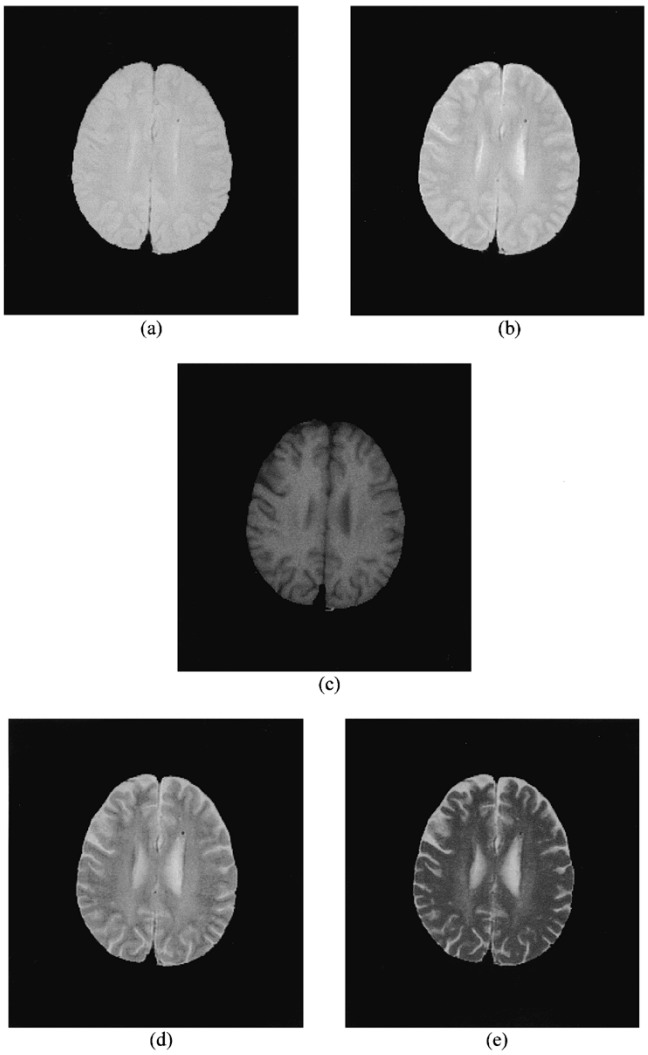

Fig. 4. Multispectral MR head images with normal physiology: (a) $\mathrm{TR}_1/\mathrm{TE}_1 = 2500$ ms/25 ms; (b) $\mathrm{TR}_2/\mathrm{TE}_2 = 1500$ ms/50 ms; (c) $\mathrm{TR}_3/\mathrm{TE}_3 = 500$ ms/11.9 ms; (d) $\mathrm{TR}_4/\mathrm{TE}_4 = 2500$ ms/75 ms; (e) $\mathrm{TR}_5/\mathrm{TE}_5 = 2500$ ms/100 ms.

using FCM are $\mathbf{C}_4 = [C_{41}, C_{42}] = [(-3.2000, 0), (3.2001, 0)]$ if point 12 was removed and clustering the remained 11 points into 2 classes. The Euclidean distances between centroids $\mathbf{C}_4$ and $\mathbf{C}_1, \mathbf{C}_2, \mathbf{C}_3$ are $\mathbf{dis}_{41} = \mathrm{distance}(\boldsymbol{C}_4, \boldsymbol{C}_1) = [0.3138, 0.3134]$, $\mathbf{dis}_{42} = \mathrm{distance}(\boldsymbol{C}_4, \boldsymbol{C}_2) = [0.3054, 0.3052]$ and $\mathbf{dis}_{43} = \mathrm{distance}(\boldsymbol{C}_4, \boldsymbol{C}_3) = [0.2702, 0.2657]$ individually. From these results, the centroids resulted from FPHN are more weakly influenced by point 12 than FCM and FHNN. Table II shows the indices of the 12 points sorted by typicality values in each cluster. Same as the results in the FPCM, points 1–5 are most typical to cluster 1 and points 7–11 are also most typical to cluster 2. Point 6 has equal typicality values to both clusters. Although point 12 also occupies equal typicality values to both clusters, it is an order of magnitude smaller than the typicality value for point 6 that means point 6 belongs to both clusters with proper grades more strongly than point 12. This also means that the FPHN can prune outliers from the data to reduce the effects of noise.

The second example is multispectral image classification in MR head images of a normal physiology shown in Fig. 4. Due to the noise in acquisition and of the partial volume effects from the low resolution of sensors, the uncertainty is widely present in medical images. The unsupervised approaches based on fuzzy clustering

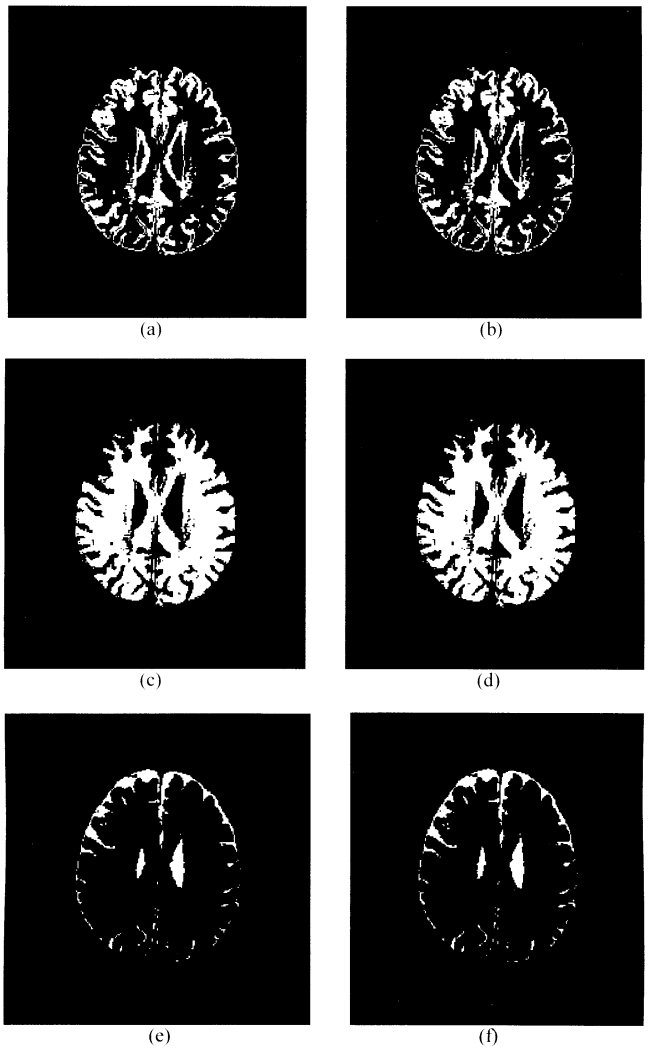

Fig. 5. Classified images in channel 5 with $\mathrm{TR}_5/\mathrm{TE}_5 = 2500\ \mathrm{ms}/100\ \mathrm{ms}$: pictures (a) GM, (c) WM, and (e) CSF are classified by FPHN; (b) GM, (d) WM, and (f) CSF are classified using FHNN, respectively.

techniques are particularly suitable for handling a decision making process in classification of multi-modal medical images. These real medical images in Figs. 4 and 9 are acquired with T_2-weighted sequences for channel images $\mathrm{CH} = 1, 2, 4$, and 5 and T_1-weighted signal for channel image $\mathrm{CH} = 3$ respectively. The acquisition parameters with different repetition time (TR) and echo time (TE) are $\mathrm{TR}_1/\mathrm{TE}_1 = 2500\ \mathrm{ms}/25\ \mathrm{ms}$, $\mathrm{TR}_2/\mathrm{TE}_2 = 1500\ \mathrm{ms}/50\ \mathrm{ms}$, $\mathrm{TR}_3/\mathrm{TE}_3 = 500\ \mathrm{ms}/11.9\ \mathrm{ms}$, $\mathrm{TR}_4/\mathrm{TE}_4 = 2500\ \mathrm{ms}/75\ \mathrm{ms}$, and $\mathrm{TR}_5/\mathrm{TE}_5 = 2500\ \mathrm{ms}/100\ \mathrm{ms}$ for Fig. 4; and $\mathrm{TR}_1/\mathrm{TE}_1 = 2500\ \mathrm{ms}/25\ \mathrm{ms}$, $\mathrm{TR}_2/\mathrm{TE}_2 = 2500\ \mathrm{ms}/50\ \mathrm{ms}$, $\mathrm{TR}_3/\mathrm{TE}_3 = 500\ \mathrm{ms}/20\ \mathrm{ms}$, $\mathrm{TR}_4/\mathrm{TE}_4 = 2500\ \mathrm{ms}/75\ \mathrm{ms}$, and $\mathrm{TR}_5/\mathrm{TE}_5 = 2500\ \mathrm{ms}/100\ \mathrm{ms}$ for Fig. 9 individually. Therefore, a training vector consisting of 5 components is directly fed into a row of the FPHN.

In Fig. 5, different regions were classified by the FPHN and FHNN from Fig. 4 such as background (BKG), gray matter (GM), white matter (WM), and cerebral spinal fluid (CSF), respectively. The classified tissues generated by FPHN and FHNN are shown in Fig. 5. In order to compare the performance of the proposed FPHN with HCM and FHNN, the computation time and number of iterations needed to classify one MR-image using the interpreter language of MATLAB are displayed in Table III. In the results, the HCM needs less iterations and computation time than the other two fuzzy approaches in average. On the other hand, the FHNN requires more iterations and computation time than the proposed FPHN although the mathematic structure of FPHN is more complex.

TABLE III
AVERAGE ITERATIONS AND COMPUTATION TIME NEEDED TO CLASSIFY ONE MR-IMAGE FOR HCM, FHNN AND THE PROPOSED FPHN

	HCM	FHNN	FPHN
iterations	12	26	15
Computation Time (sec.)	16	31	22

TABLE IV
UNIFORMITY MEASURES IN VARIANT CHANNELS USING THE DIFFERENT METHODS FOR FIG. 4

Methods \ Channels		*CH* 1	*CH* 2	*CH* 3	*CH* 4	*CH* 5	Average
HCM	4 regions	0.9868	0.9873	0.9875	0.9875	0.9863	0.9870
	5 regions	0.9882	0.9869	0.9877	0.9885	0.9878	0.9878
FHNN	4 regions	0.9946	0.9964	0.9977	0.9974	0.9959	0.9964
	5 regions	0.9977	0.9972	0.9977	0.9969	0.9966	0.9972
FPHN	4 regions	0.9953	0.9968	0.9979	0.9976	0.9965	0.9968
	5 regions	0.9978	0.9973	0.9977	0.9969	0.9965	0.9972

The uniformity measure adopted from Levine and Nazif [28] is used to show the classification performance for the classified regions compared the proposed FPHN with HCM and FHNN in this paper. In digital images, the uniformity of a feature over a region is inversely proportional to the variance of the value of that feature evaluated at every pixel belonging to that region. For a given-segmented image, the uniformity measure UM_α is given by

$$\mathrm{UM}_\alpha = 1 - \left(\frac{\sum_{R_i \in \alpha} p_i \sigma_i^2}{M} \right) \tag{17}$$

where R_i is the segmented region i, P_i is the weight associated with the contribution of region R_i to the measure. The value is computed as

$$M = \left(\sum_{R_i \in \alpha} p_i \right) \cdot \frac{(f_{\max} - f_{\min})^2}{2} \tag{18}$$

with $f_{\max}$ = maximum gray level and $f_{\min}$ = minimum gray level in the image respectively. If A_i is the total number of pixels in region R_i for class i, the variance for gray levels in R_i is defined as

$$\sigma_i = \sum_{(x,y) \in R_i} \frac{[f(x,y) - \bar{f}_i]^2}{A_i} \tag{19}$$

where $f(x, y)$ represents the gray level of pixel (x, y), $\bar{f}_i$ is the average gray level in region R_i. The classification performance is more promising as the uniformity measure is closer to 1 for a segmented image. Although Fig. 5 almost displays the similar classified results in subjective observation, the uniformity measures shown in Table IV indicates more promising results can be obtained by the FPHN. From Tables III and IV, the FPHN can obtain more uniform classification than the HCM algorithm and obtain better performance than FHNN. Additionally, the better uniformity measure can be obtained with more regions than those yielded by fewer regions.

In order to emphasize the classification ability of the proposed FPHN, several test phantoms were constructed for simulation. Every test phantom was made up of six overlapping ellipses. Each ellipse

TABLE V
SIMULATING CLUSTER CENTERS OF DIFFERENT OBJECTS FOR VARIANT CHANNELS IN TEST PHANTONS WHICH ARE THE AVERAGE VALUES ESTIMATED FROM TEN MULTISPECTRAL MR HEAD IMAGES WITH NORMAL PHYSIOLOGY USING THE SAME PARAMETERS IN FIG. 4

Channels / Objects	*CH* 1	*CH* 2	*CH* 3	*CH* 4	*CH* 5
BKG	0	0	0	0	0
GM	192	183	91	152	108
WM	166	159	103	108	75
CSF	203	248	68	220	199

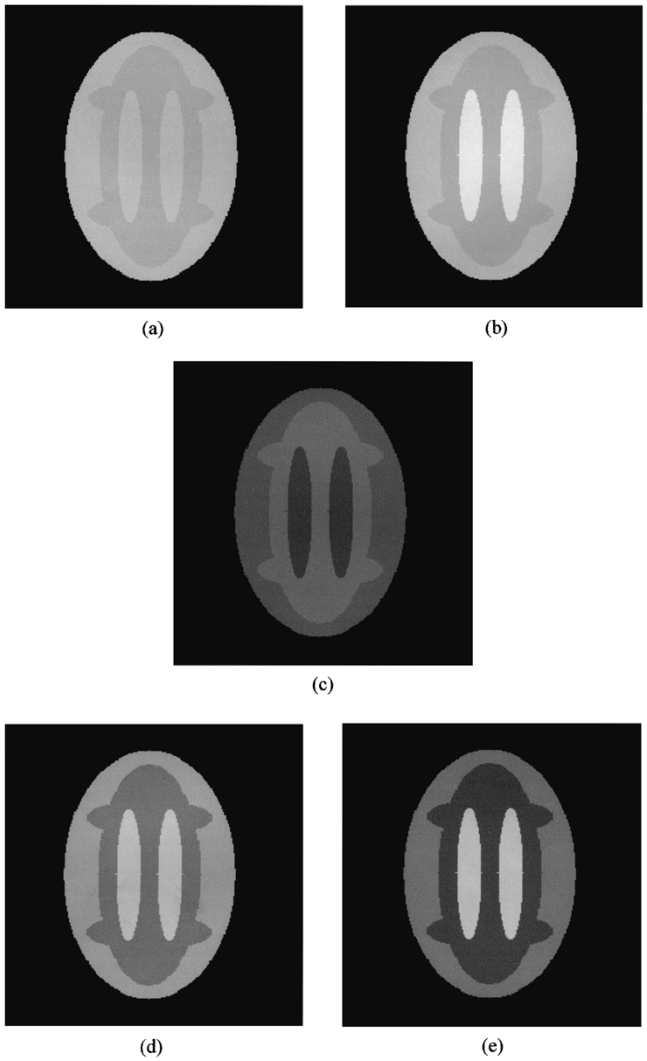

Fig. 6. Test phantoms for simulating different objects (BKG, WM, GM, and CSF) in multispectal image.

represents one structural area of tissue. From periphery to the center, they were the background (BKG, 41 500 pixels), gray matter (GM, 10 270 pixels), white matter (WM, 10 116 pixels), and cerebrospinal fluid (CSF, 3650 pixels), respectively. The cluster centers for different channels in test phantoms, in Table V, are the average values estimated from ten sets of multispectral MR head images with normal physiology using the same parameters in Fig. 4. The computer-generated images to simulate variant channels are shown in Fig. 6. In addition, a Gaussian-distribution noise with gray levels ranging from $-\delta$ to $+\delta$

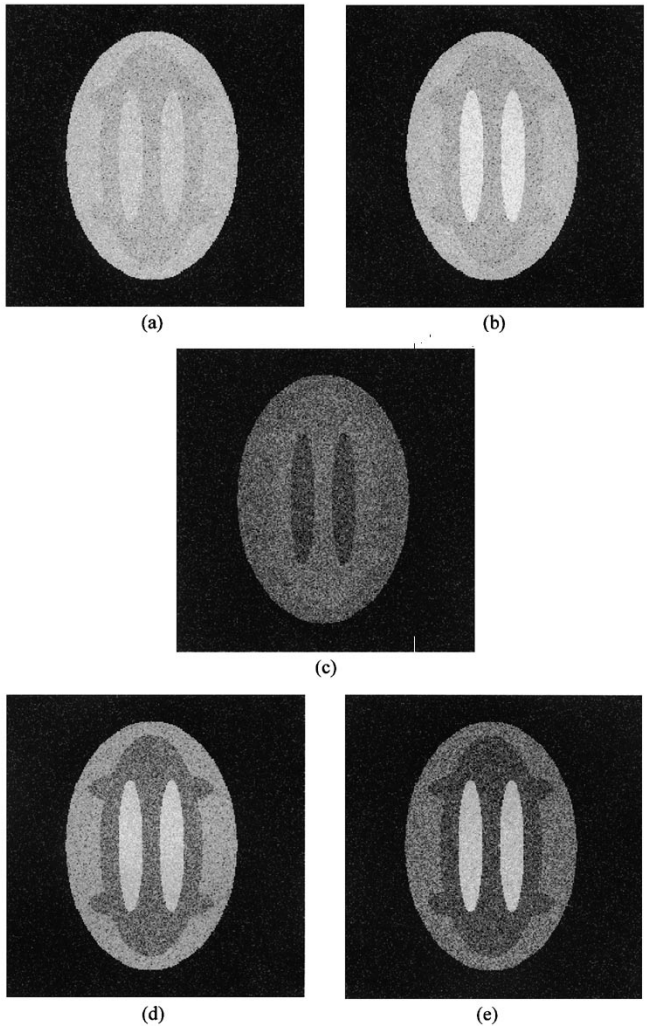

Fig. 7. Test phantoms for simulating different objects (BKG, WM, GM, and CSF) in multispectal image with adding Gaussian noise $\delta = \pm 30$.

TABLE VI
SEGMENTATION PERFORMANCES IN CORRECT DETECTING PIXELS FOR FHNN AND FPHN METHODS USING THE SIMULATED IMAGE WITH $\delta = \pm 25$

Simulation object	Actual pixels	FHNN	FPHN
Background(BKG)	41500	41500(100%)	41500(100%)
GM	10270	9647(93.9%)	9615(93.6%)
WM	10116	9372(92.6%)	9422(93.1%)
CSF	3650	3650(100%)	3650(100%)
Misclassified pixels	0	1367	1349
Average correct ratio		96.6%	96.7%

TABLE VII
SEGMENTATION PERFORMANCES IN CORRECT DETECTING PIXELS FOR FHNN AND FPHN METHODS USING THE SIMULATED IMAGE WITH $\delta = \pm 30$

Simulation object	Actual pixels	FHNN	FPHN
Background(BKG)	41500	41500(100%)	41500(100%)
GM	10270	9317(90.7%)	9220(89.8%)
WM	10116	8775(86.7%)	8889(87.9%)
CSF	3650	3646(99.9%)	3646(99.9%)
Misclassified pixels	0	2298	2281
Average correct ratio		94.3%	94.4%

TABLE VIII
SEGMENTATION PERFORMANCES IN CORRECT DETECTING PIXELS FOR FHNN AND FPHN METHODS USING THE SIMULATED IMAGE WITH $\delta = \pm 50$

Simulation object	Actual pixels	FHNN	FPHN
Background(BKG)	41500	41197(99.3%)	41197(99.3%)
GM	10270	7787(75.8%)	7749(75.5%)
WM	10116	7280(72.0%)	7377(72.9%)
CSF	3650	3527(96.6%)	3513(96.2%)
Misclassified pixels	0	5747	5700
Average correct ratio		85.9%	86.0%

TABLE IX
SEGMENTATION PERFORMANCES IN CORRECT DETECTING PIXELS FOR FHNN AND FPHN METHODS USING THE SIMULATED IMAGE WITH $\delta = \pm 80$

Simulation object	Actual pixels	FHNN	FPHN
Background(BKG)	41500	33231(80.1%)	39220(94.5%)
GM	10270	7678(74.8%)	5970(58.1%)
WM	10116	1844(18.2%)	4721(46.7%)
CSF	3650	3289(90.1%)	3147(86.2%)
Misclassified pixels	0	19494	12478
Average correct ratio		65.8%	71.4.0%

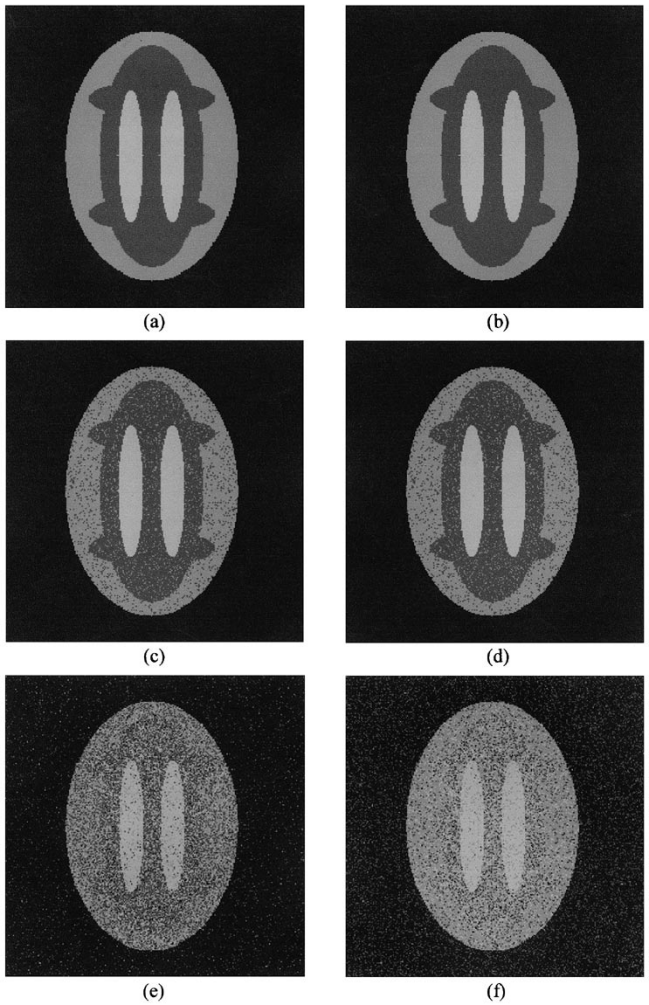

Fig. 8. Classified images with variant Gaussian noises: pictures (a) $\delta = \pm 10$, (c) $\delta = \pm 30$, and (e) $\delta = \pm 80$ are classified by FPHN; (b) $\delta = \pm 10$, (d) $\delta = \pm 30$, and (f) $\delta = \pm 80$ are classified using FHNN respectively.

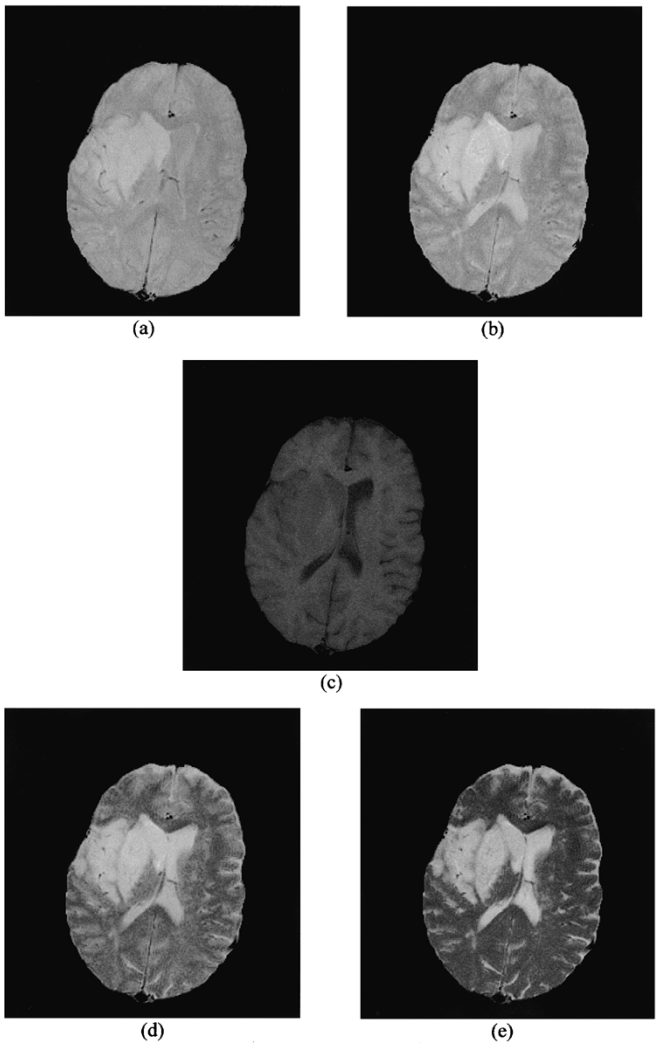

Fig. 9. Multispectral MR head images with cerebral infarction: (a) $\mathrm{TR}_1/\mathrm{TE}_1 = 2500\,\mathrm{ms}/25\,\mathrm{ms}$; (b) $\mathrm{TR}_2/\mathrm{TE}_2 = 2500\,\mathrm{ms}/50\,\mathrm{ms}$; (c) $\mathrm{TR}_3/\mathrm{TE}_3 = 500\,\mathrm{ms}/20\ \mathrm{ms}$; (d) $\mathrm{TR}_4/\mathrm{TE}_4 = 2500\,\mathrm{ms}/75\ \mathrm{ms}$; (e) $\mathrm{TR}_5/\mathrm{TE}_5 = 2500\,\mathrm{ms}/100\,\mathrm{ms}$.

was added to test phantoms. The test phantoms with Gaussian -distribution noise $\delta = \pm 30$ for different channels are shown in Fig. 7. The classified results of test phantoms with variant noises $\delta = \pm 25, \pm 30, \pm 50$ and ± 80 are displayed in Tables VI, VII, VIII and IX respectively. The simulated structural areas of tissues can be completely and correctly classified when the Gaussian noise is $|\delta| \leq 10$ for both FPHN and FHNN. In these Tables, the proposed FPHN can obtain more promising classification than the FHNN. For example, 9372 pixels were detected with a 92.6% correct rate using FHNN while 9422 pixels were classified with 93.1% correct rate using the FPHN with $\delta = \pm 25$. The total misclassified pixels for the test phantoms with $\delta = \pm 25$ were 1367 and 1349 using FHNN and the proposed FPHN, respectively. The better classification rates can be clearly displayed by the FPHN than those yielded by the FHNN in more noises. The classified regions in different images for variant noises are shown in Fig. 8.

The fourth example is multispectral images classification in MR head images of a patient diagnosed with cerebral infarction shown in Fig. 9. Fig. 10 shows the five regions BKG, GM, WM, CSF, and cerebral infarction (CI) classified by the FPHN respectively. After a post processing with median filtering, the detail of an abnormal region with cerebral infarction is displayed in of Fig. 10(e).

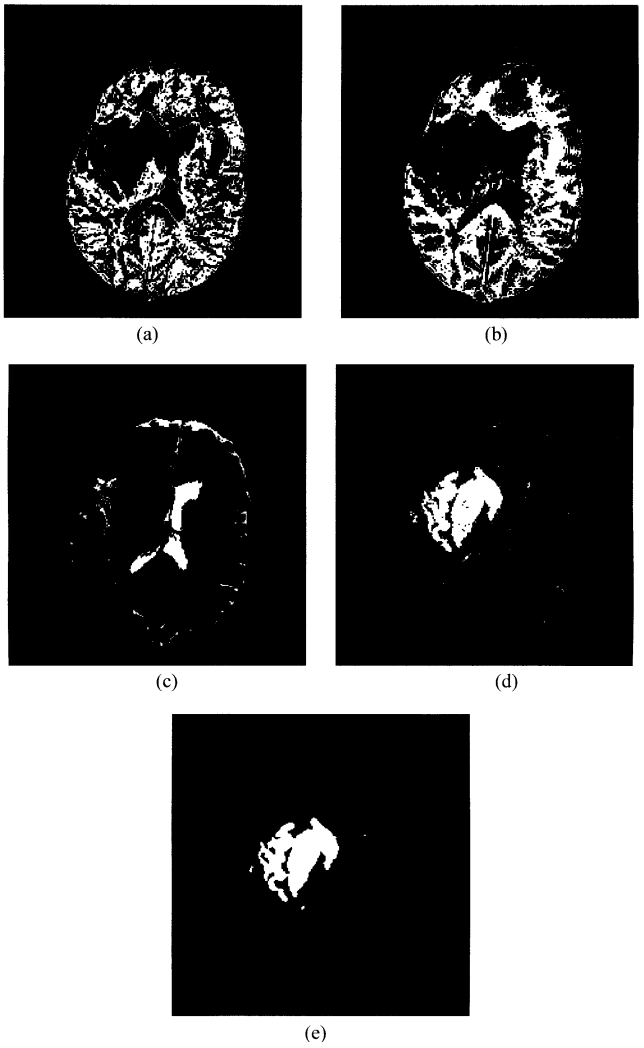

Fig. 10. Classified images using the proposed FPHN in channel 2 with $\mathrm{TR}_2/\mathrm{TE}_2 = 2500$ ms$/50$ ms: (a) GM; (b) WM; (c) CSF; (d) CI; and (e) CI after median filter.

V. Discussion and Conclusions

A modified Hopfield-net model called fuzzy possibilistic Hopfield net (FPHN) embedded fuzzy possibilistc c-means strategy with 2 neuron states, membership state and typicality state, is proposed to the classification of multispectral images. From the simulations, the proposed FPHN seems to solve the noise sensitivity fault of fuzzy c-means and overcoming the simultaneous clustering problem of possibilistic c-means strategy. Therefore, the FPHN can prune outliers from the data to reduce the effects of noise. From the experimental results, the FPHN can classify more suitable regions than HCM and FHNN methods in the application of multispectral images and the generated phantoms classification. Moreover, the designed FPHN neural-network-based approach with a fuzzy reasoning has simple features and clear potential for optimal problems.

Acknowledgment

This work was supported by the National Science Council, Taiwan, R.O.C., under Grants NSC89-2218-E-167-001 and NSC90-2213-E-167-003. The authors would like to thank the anonymous reviewers whose constructive comments greatly improved the presentation of the paper.

References

[1] M. Vannier, T. Pilgram, C. Speidel, L. Neumann, D. Rickman, and L. Schertz, "Validation of magnetic resonance imaging (MRI) multispectral tissue classification," *Comp. Med. Imag. Graph.*, vol. 15, pp. 217–228, 1991.

[2] C.-I. Chang and C. Brumbley, "A kalman filtering approach to multispectral image classification and detection of changes in signature abundance," *IEEE Trans. Aerosp. Electron. Syst.*, vol. 37, pp. 257–268, 1999.

[3] A. Ifarraguerri and C.-I. Chang, "Multispectral and hyperspectral image analysis with convex cones," *IEEE Trans. Geosci. Remote Sensing*, vol. 37, pp. 756–770, 1999.

[4] T. Taxt and A. Lundervold, "Multispectral analysis of the brain using magnetic resonance imaging," *IEEE Trans. Med. Imag.*, vol. 13, pp. 470–481, 1994.

[5] M. W. Vannier, R. L. Butterfield, D. Jordan, W. A. Murphy, R. G. Levitt, and M. Gado, "Multispectral analysis of magnetic resonance images," *Radiology*, vol. 154, pp. 221–224, 1985.

[6] M. Ozkan, B. M. Dawant, and R. J. Maciunas, "Neural-network-based segmentation of muliti-modal medical images: A comparative and prospective study," *IEEE Trans. Med. Imag.*, vol. 12, pp. 534–544, 1993.

[7] J.-S. Lin, K.-S. Cheng, and C.-W. Mao, "Segmentation of multispectral magnetic resonance images using penalized fuzzy competitive learning network," *Comp. Biomed. Res.*, vol. 29, pp. 314–326, 1996.

[8] ——, "Multispectral magnetic resonance images segmentation using fuzzy Hopfield neural network," *Int. J. Bio-Med. Comput.*, vol. 42, pp. 205–214, 1996.

[9] G. H. Ball and D. J. Hall, "A clustering technique for summarizing multivariate data," *Behav. Sci.*, vol. 12, pp. 153–155, 1967.

[10] J. C. Dunn, "A fuzzy relative of the ISODATA process and its use in detecting compact well-separated clusters," *J. Cybern.*, vol. l.3, pp. 32–57, 1974.

[11] H. J. Zimmermann, *Fuzzy Set Theory and Its Application.* Boston, MA: Kluwer, 1991.

[12] M. A. Ismail and S. Z. Selim, "Fuzzy c-mean: Optimality of solutions and effective termination of the algorithm," *Pattern Recog.*, vol. 19, pp. 481–485, 1986.

[13] J. C. Bezdek, "Fuzzy Mathematics in Pattern Classification," Ph.D. Dissertation, Dept. App. Math., Cornell Univ., Ithaca, NY, NY, 1973.

[14] M. S. Yang, "On a class of fuzzy classification maximum likelihood procedures," *Fuzzy Sets Syst.*, vol. 57, pp. 365–375, 1993.

[15] M. S. Yang and C.-F. Su, "On parameter estimation for normal mixtures based on fuzzy clustering algorithms," *Fuzzy Sets Syst.*, vol. 68, pp. 13–28, 1994.

[16] J.-S. Lin, "Fuzzy clustering using a compensated fuzzy Hopfield network," *Neural Proces. Lett.*, vol. 10, pp. 35–48, 1999.

[17] R. Krishnapuram and J. M. Keller, "A possibilistic approach to clustering," *IEEE Trans. Fuzzy Syst.*, vol. 1, pp. 98–110, 1993.

[18] ——, "The possibilistic c-means algorithm: Insights and recommendations," *IEEE Trans. Fuzzy Syst.*, vol. 4, pp. 385–393, 1996.

[19] N. R. Pal, K. Pal, and J. C. Bezdek, "A mixed c-means clustering model," in *IEEE Int. Conf. Fuzzy Syst.*, vol. 1, 1997, pp. 11–21.

[20] A. Kanstein, M. Thomas, and K. Goser, "Possibilistic reasoning neural network," in *IEEE Int. Conf. Neural Networks*, vol. 4, 1997, pp. 2541–2545.

[21] J. C. Bezdek, L. O. Hall, and L. P. Clarke, "Review of MR image segmentation techniques using pattern recognition," *Med. Phys.*, vol. 20, pp. 1033–1048, 1993.

[22] R. N. Dave and R. Krishnapuram, "Robust clustering methods: A unified review," *IEEE Trans. Fuzzy Syst.*, vol. 5, p. AU: PAGE #'S, 1997.

[23] J. J. Hopfield, "Neural networks and physical systems with emergent collective computational abilities," in *Proc. Nat. Acad. Sci.*, vol. 79, USA, 1982, pp. 2554–2558.

[24] J. J. Hopfield and D. W. Tank, "Neural computation of decisions in optimization problems," *Biol. Cybern.*, vol. 52, pp. 141–152, 1985.

[25] J.-S. Lin and S.-H. Liu, "A competitive continuous Hopfield neural network for vector quantization in image compression," *Eng. Applicat. Artif. Intell.*, vol. 12, pp. 111–118, 1999.

[26] J.-S. Lin, K.-S. Cheng, and C.-W. Mao, "A fuzzy Hopfield neural network for medical image segmentation," *IEEE Trans. Nucl. Sci.*, vol. 43, pp. 2389–2398, 1996.

[27] D.-C. Cheng, Q. Pu, K.-S. Cheng, and H. Burkhardt, "Possibilistic Hopfield neural network on CT brain hemorrhage image segmentation," in *Proc. of the 4th Asian Conf. on Computer Vision*, vol. II, 2000, pp. 871–876.

[28] M. D. Levine and A. M. Nazif, "Dynamic measurement of computer generated image segmentations," *IEEE Trans. Pattern Anal. Machine Intell.*, vol. PAMI-7, pp. 156–164, 1985.